Matching material and cellular timescales maximizes cell spreading on viscoelastic substrates

Ze Gong[a,b,c], Spencer E. Szczesny[d], Steven R. Caliari[e,f,g], Elisabeth E. Charrier[h], Ovijit Chaudhuri[i], Xuan Cao[a,c], Yuan Lin[b,1], Robert L. Mauck[c,d], Paul A. Janmey[c,h], Jason A. Burdick[c,g], and Vivek B. Shenoy[a,c,g,1]

[a]Department of Materials Science and Engineering, University of Pennsylvania, Philadelphia, PA 19104; [b]Department of Mechanical Engineering, University of Hong Kong, Hong Kong, China; [c]Center for Engineering Mechanobiology, University of Pennsylvania, Philadelphia, PA 19104; [d]McKay Orthopaedic Research Laboratory, Department of Orthopaedic Surgery, Perelman School of Medicine, University of Pennsylvania, Philadelphia, PA 19104; [e]Department of Chemical Engineering, University of Virginia, Charlottesville, VA 22904; [f]Department of Biomedical Engineering, University of Virginia, Charlottesville, VA 22904; [g]Department of Bioengineering, University of Pennsylvania, Philadelphia, PA 19104; [h]Institute for Medicine and Engineering, University of Pennsylvania, Philadelphia, PA 19104; and [i]Department of Mechanical Engineering, Stanford University, Stanford, CA 94305

Edited by David A. Weitz, Harvard University, Cambridge, MA, and approved February 5, 2018 (received for review September 21, 2017)

Recent evidence has shown that, in addition to rigidity, the viscous response of the extracellular matrix (ECM) significantly affects the behavior and function of cells. However, the mechanism behind such mechanosensitivity toward viscoelasticity remains unclear. In this study, we systematically examined the dynamics of motor clutches (i.e., focal adhesions) formed between the cell and a viscoelastic substrate using analytical methods and direct Monte Carlo simulation. Interestingly, we observe that, for low ECM rigidity, maximum cell spreading is achieved at an optimal level of viscosity in which the substrate relaxation time falls between the timescale for clutch binding and its characteristic binding lifetime. That is, viscosity serves to stiffen soft substrates on a timescale faster than the clutch off-rate, which enhances cell–ECM adhesion and cell spreading. On the other hand, for substrates that are stiff, our model predicts that viscosity will not influence cell spreading, since the bound clutches are saturated by the elevated stiffness. The model was tested and validated using experimental measurements on three different material systems and explained the different observed effects of viscosity on each substrate. By capturing the mechanism by which substrate viscoelasticity affects cell spreading across a wide range of material parameters, our analytical model provides a useful tool for designing biomaterials that optimize cellular adhesion and mechanosensing.

mechanotransduction | viscoelasticity | cell spreading | focal adhesion | timescales

Mounting evidence has demonstrated that cells can sense and react to the physical properties of the extracellular matrix (ECM), an ability that plays a key role in processes such as cell migration (1–3), spreading (4, 5), and proliferation (6–8). It is commonly believed that focal adhesions (FAs), which anchor the cell to the ECM as well as serving as hubs for the exchange of biological and mechanical stimuli (9, 10), are responsible for such mechanosensitivity of cells.

It has been recognized that cells probe the stiffness of their surroundings by gauging the resistance of FAs to actin retrograde flow generated by intracellular myosin contractions (11–14). FAs, acting like molecular clutches, alter the movement of actin intracellular structures by providing a tunable connection to the ECM (13, 15). Based on this picture, the well-known motor-clutch model (15–17) was developed, which predicted a biphasic dependence of cell adhesion traction (and consequently cell spreading) on ECM rigidity. However, recent experiments have found a monotonic increase of cell spreading with the ECM rigidity (18, 19), which can be attributed to reinforcement mechanisms including, for example, the activation of adhesion proteins under high surrounding stiffness/load level or the recruitment of integrins into the FAs (20, 21).

Beyond substrate rigidity, most natural ECM materials such as collagen, fibrin (22), and tissues (23–25) are viscoelastic in nature and exhibit a strong frequency-dependent mechanical response. Interestingly, it was reported recently that cell spreading can be enhanced by stress relaxation of a cell culture substrate (e.g., alginate, polyacrylamide), which was dependent on the elastic modulus of the substrate (4, 26). This was explained by local remodeling (leading to increased ligand density) of the matrix during deformation (4), which corresponds to a plastic rather than viscous response. On the other hand, our own experiments (to be discussed in *Model Predicts Cells Spreading for Several Different Cell Types Across a Wide Range of Elastic and Viscous Substrate Properties*) suggest that viscosity has a negligible effect on how cells spread. However, it is unclear how a purely viscoelastic substrate can have different effects on cell spreading, largely due to the lack of a theoretical model capable of revealing the physical mechanisms governing the cellular response to viscoelasticity.

To address this critical issue, we systematically examined how cell spreading is influenced by the viscoelastic components of the ECM via an analytical mean-field analysis and direct Monte Carlo simulations. Specifically, by treating the ECM as a standard linear viscoelastic solid, we found that an intermediate level of viscosity can promote cell spreading when the ECM rigidity is relatively low, reflecting the fact that the substrate relaxation time under such circumstance falls between the timescale

Significance

It is well known that cell proliferation, differentiation, and migration depend strongly on the mechanical stiffness of the extracellular matrix (ECM). Natural ECMs also exhibit dissipative (i.e., plastic, viscoelastic) properties, which can modulate cellular behavior. However, to fully utilize this information in bioengineering applications, a systematic understanding of the role of substrate viscosity on cell function is needed. Using combined theoretical and experimental approaches, we demonstrated that viscous dissipation can be as important as elasticity in determining cell response. Specifically, we found that intermediate viscosity maximizes cell spreading on soft substrates, while cell spreading is independent of viscosity on stiff substrates. This information can now be used to design dissipative biomaterials for optimal control of cell behavior.

Author contributions: V.B.S. designed research; Z.G., S.R.C., E.E.C., and O.C. performed research; Z.G., S.E.S., X.C., R.L.M., P.A.J., and J.A.B. analyzed data; Z.G., S.E.S., Y.L., and V.B.S. wrote the paper; and S.R.C., E.E.C., and O.C. conducted the experiments.

The authors declare no conflict of interest.

This article is a PNAS Direct Submission.

[1]To whom correspondence may be addressed. Email: vshenoy@seas.upenn.edu or ylin@hku.hk.

This article contains supporting information online at www.pnas.org/lookup/suppl/doi:10.1073/pnas.1716620115/-/DCSupplemental.

Published online March 5, 2018.

for clutch binding and its characteristic binding lifetime. That is, viscosity serves to stiffen soft substrates, which enhances cell–ECM adhesion and cell spreading. As for high rigidity, the large tension borne by the clutches triggers an increase in their binding rates as well as an increase in the integrin density (clutch reinforcement), which saturates the cell response to substrate stiffness and eliminates any role of viscosity. These data are presented in heat maps of spreading response in the parameter space spanned by the substrate and cellular timescales.

Our theoretical predictions that incorporate the viscoelastic relaxation time spectrum analysis are in excellent agreement with previous observations as well as providing the basis for understanding our own experiments where ECMs with tunable viscoelastic properties were fabricated by two different methods. By capturing the mechanism by which substrate viscoelasticity affects cell spreading across a wide range of material parameters, our analytical model provides a useful tool for designing biomaterials that optimize cellular adhesion and mechanosensing.

Model Description

The canonical motor-clutch model (15), as schematically illustrated in Fig. 1*A*, was adopted to study the impact of viscoelasticity on spreading. In this model, myosin motors pull the actin filament bundle toward the cell center, generating retrograde flow of actin. On the other hand, the molecular bonds/clutches, connecting the F-actin with the substrate, were assumed to be able to randomly break or reengage with a dissociation or association rate of $r_{off,i}$ or r_{on}, respectively. Engagement of the clutches leads to slowing down of the retrograde flow, allowing the polymerization at the leading edge to push the cell membrane forward, resulting in the spreading of the cell. The master equation describing the evolution of the state of each clutch can be written as

$$\frac{dP_{b,i}}{dt} = (1 - P_{b,i}) r_{on} - P_{b,i}\, r_{off,i}, \qquad [1]$$

where $P_{b,i}$ represents the probability for clutch i to remain engaged. As the F-actin slides, a bound clutch (treated as a linear spring with stiffness, k_c) undergoes stretching and hence generates a force $F_{c,i}$ resisting the retrograde flow of actin. If the displacements of the filament end and substrate end of the clutch are denoted as $x_{c,i}$ and x_s, then the force can be expressed as $F_{c,i} = k_c(x_{c,i} - x_s)$. Using a Bell model (27), the dissociation rate is expected to increase exponentially with $F_{c,i}$; that is, $r_{off,i} = r_{off}^0 \cdot \exp(F_{c,i}/F_b)$, where F_b is a characteristic force and r_{off}^0 represents the breaking rate of clutches in the absence of any force. Recent experiments demonstrated that FAs grow on stiff substrates through the recruitment of integrins to the adhesion complex via talin unfolding (20, 21). Following the model developed by Elosegui-Artola et al. (21) that describes such FA reinforcement, the association rate r_{on} is replaced by $r_{on}^0(1 + \alpha(F_a - F_{cr}))$ once the average clutch force F_a has surpassed a force threshold F_{cr} (refer to *Supporting Information* for more details). A value of 0.2 per piconewton was chosen for α based on fits of cellular spreading on purely elastic substrates (Fig. S7).

While many viscoelastic substrates possess multiple relaxation times, we chose to represent the substrate as a standard linear viscoelastic material for two main reasons (Fig. 1*A*). First, this model captures the essential effects of the competition between the viscoelastic timescale of the substrate and the intrinsic cellular timescales and allows us to identify the impact of different mechanical parameters (long-term and additional stiffness). Second, by fitting our experimental relaxation data to a Prony series (i.e., the generalized Maxwell model with multiple timescales) and carrying out simulations of spreading using this model (*Simulation with Multiple Relaxation Timescales* and Fig. S8), we found that only one relaxation time significantly affects the spreading behavior. This single relaxation time constant was determined using the time spectrum analysis, which is described in *Results*. The force–displacement relation of standard linear viscoelastic model is given by

$$(k_a + k_l)\eta \frac{dx_s}{dt} + k_a k_l x_s = k_a F_s + \eta \frac{dF_s}{dt}. \qquad [2]$$

Here k_a and k_l are the additional and long-term stiffness, respectively, of substrate, while η represents the viscosity for dashpot (Fig. 1*A*). The total load transmitted to the substrate F_s is the sum of all forces sustained by bounded clutches; that is,

$$F_s = k_c \sum_{i=1}^{n_c} (x_{c,i} - x_s). \qquad [3]$$

On the other hand, the substrate force can be related to the retrograde flow speed, V_f, through the Hill relation (15)

$$V_f = v_u \cdot \left[1 - \frac{F_s}{N_m F_m}\right], \qquad [4]$$

where N_m is the number of myosin motors, F_m refers to the characteristic stalling force, and v_u represents the maximum retrograde flow velocity. For a clutch that remains engaged, its filament end moves with the F-actin. In comparison, since a broken clutch carries zero load and moves with the substrate, we can effectively set $x_{c,i} = x_s$. Consequently, on average, the moving velocity of the filament end of a clutch can be expressed as

$$\frac{dx_{c,i}}{dt} = P_{b,i} V_f + (1 - P_{b,i}) \frac{dx_s}{dt}. \qquad [5]$$

To connect this analysis with cell spreading, we recall that cells spread via lamellipodia, flat sheet-like structures driven by the actin polymerization-induced protrusive forces (pushing against the cell membrane) (28). During spreading, actin monomers flow from the cell center to the edge to sustain continuous polymerization and offset the retrograde flow of F-actin (29–31). Importantly, it has been found that the sum of the retrograde flow velocity and the speed of actin protrusion remains approximately constant (5, 30, 31). Based on these observations, we were able to relate the cell spreading speed, V_s, to the retrograde flow (V_f) and polymerization velocity (V_p, treated as a constant) as

$$V_s = V_p - V_f. \qquad [6]$$

Here, it should be noted that the spreading velocity V_s is the initial spreading speed when the cells are seeded on the substrates. After this initial phase of polymerization, outward motion of the actin filaments will be countered not only by rearward forces from the myosin motors but also by the resistance of the plasma membrane, eventually leading to a steady-state configuration where the cell spreading area becomes constant (Fig. S2). This steady-state spreading area is a function of the initial spreading velocity, initial spreading radius, and the properties of the cytoskeleton and cell membrane (*Initial Spreading Speed Determines the Final Spreading Area*). Kinetic Monte Carlo (KMC) simulations show that, given the initial radius and cytoskeleton properties, the steady-state spreading radius increases in an almost linear manner with respect to the initial spreading speed (Fig. S2).

From Eqs. **1**–**6**, the dynamic behavior of the molecular clutches as well as of cell spreading can be simulated by a KMC method (15). In addition, a mean-field approach can also be applied (see *Supporting Information* for details) to examine the problem in an analytical manner. In this case, the behaviors of all clutches are averaged into a single "ensemble" clutch with effective stiffness $k_c n_c P_b$, where P_b is the fraction of clutches that

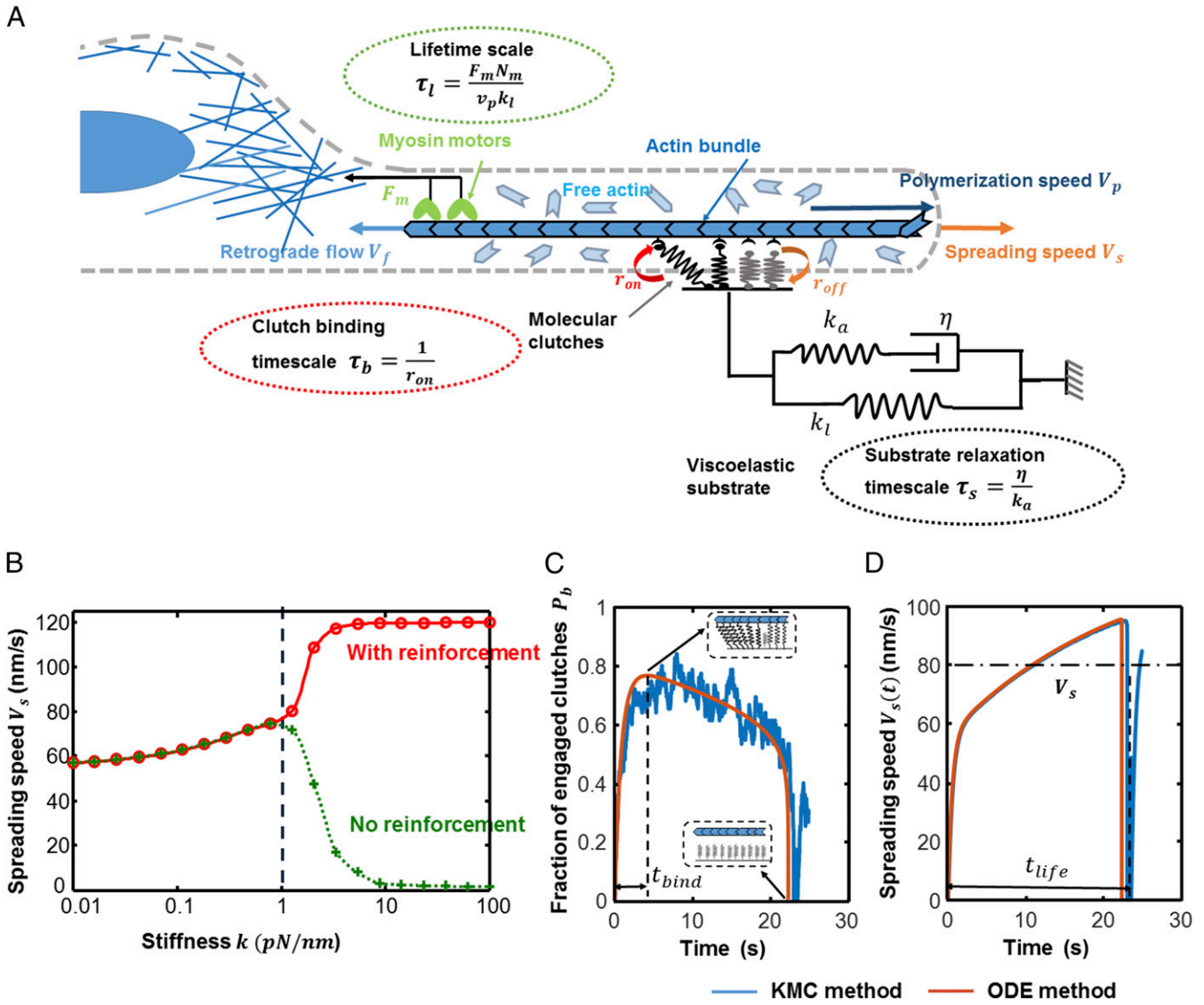

Fig. 1. Modified motor-clutch model investigating FA and cell spreading behavior on viscoelastic substrates. (*A*) Schematic of the motor-clutch model of a cell attached to a viscoelastic substrate represented as a standard linear solid. Myosin motors pull the actin bundle toward cell center at a retrograde flow velocity, V_f. Clutches connect the actin bundle to the substrate based on the reaction rates r_{on} and r_{off} and resist the retrograde flow. Greater resistance to the retrograde flow increases cell spreading due to polymerization of the actin bundle. Three timescales govern the model behavior: clutch binding timescale ($\tau_b = 1/r_{on}$), FA lifetime scale ($\tau_l = F_s/v_0 k_l$), and substrate relaxation timescale ($\tau_s = \eta/k_a$). (*B*) Representative cell spreading speed as a function of substrate stiffness, for a purely elastic substrate, predicted by our model. The red curve corresponds to the case where clutch is reinforced by force over a threshold level, while the green curve represents the scenario without any reinforcement. The black dashed line indicates the critical stiffness above which clutch reinforcement begins to take effect. (*C* and *D*) Results for a typical set of parameters ($k_a = 1$ pN/nm, $k_l = 0.1$ pN/nm, $\eta = 1$pN·s/nm) show that the (*C*) fraction of engaged clutches and (*D*) retrograde flow (ODE, red line) and the KMC method (blue line) are almost identical. *Insets* in *C* show whether the clutches are attached or detached. The dash-dotted line in *D* indicates the mean spreading speed over one cycle of clutch engagment and detachment.

remain engaged. By solving the corresponding ordinary differential equation (ODE) from the mean-field theory, the temporal evolution of the clutch status can be obtained. The values of parameters are given in Table S1 (more details are provided in *General Model Parameters*).

Results

Intermediate Viscosity for Soft Substrates Promote Cell Spreading. First, we consider purely elastic substrates, where our model predicts that cell spreading increases gradually with ECM stiffness and eventually saturates (Fig. 1*B*, red line). In contrast, if no reinforcement is included in the model, the spreading velocity will actually start to decrease with the ECM rigidity for stiffness higher than ∼1 pN/nm (Fig. 1*B*, green line). Since our experimental data consistently demonstrated that cells exhibit a monotonic relation between spreading area and elastic stiffness, we focused on the reinforcement case (the case without reinforcement is included in *Supporting Information* for comparison). For viscoelastic substrates, typical results from our model for single FA life cycle are shown in Fig. 1 *C* and *D*. The clutches gradually engage with the sliding filament at the beginning (Fig. 1*C*) to transmit higher traction forces, leading to an increased substrate displacement and spreading speed (Fig. 1*D*). However, after passing the binding time t_{bind} (marked in Fig. 1*C*), bounded clutches start to break as the load level inside keeps increasing. Finally, at $t = t_{\text{life}}$ (i.e., the binding lifetime for a FA marked in Fig. 1*D*), all clutches break. This produces a dynamic binding cycle that will repeat itself with a period of t_{life}, which is the same

"load and fail" response produced by other motor-clutch models (15, 16). For comparison, representative trajectories from the KMC simulations are also given in Fig. 1 *C* and *D*, which are in good agreement with the mean-field analysis. It must be pointed out that the lifetime, t_{life}, of such load and fail response would gradually increase and even diverge (i.e., stable FAs that cannot break) as the reinforcement takes effect and increases the binding rate (Fig. S1). To characterize the spreading behavior for cells, we use the mean spreading speed, V_s, calculated by averaging the speed over its lifetime (*Supporting Information*). Given the agreement between the two methods (Fig. S1*A*), the ODE solution will be applied for all following parametric studies to reveal the ensemble behavior of FAs over their lifetime.

As shown in Fig. 1*A*, the response of a substrate represented by the standard linear model is characterized by three parameters: the long-term stiffness k_l, the additional stiffness k_a, and the viscosity η. For a constant applied substrate displacement, $k_a + k_l$ represents the initial stiffness of the substrate, k_a represents the drop in stiffness as the substrate relaxes, and k_l represents the equilibrium substrate stiffness. Note that we assumed a typical FA length of 1 μm (11); therefore, a stiffness of 1 pN/nm is equivalent to a modulus of 1 kPa (*Extracting Substrate Parameters from Relaxation Test*). The heat maps of spreading speed with respect to the entire parameter space (k_a, k_l, η) are given in Fig. 2*A*.

Depending on the elastic parameters, viscosity can influence cell spreading in very different ways. When viscosity is very small ($\eta < 10^{-2}$ pN·s/nm), the response of cells is largely determined by the long-term ECM stiffness, which is similar to the case of purely elastic substrates. However, as viscosity increases, the spreading behavior is highly affected by both the long-term and additional stiffness of the substrate. Specifically, viscosity was found to promote cell spreading for soft substrates (i.e., with relatively low long-term stiffness) as it increases the effective stiffness that cells can sense, leading to maximized cell spreading at intermediate viscosity values (Fig. 2*B*). In comparison, for substrates with a large long-term stiffness ($k_l > 5$ pN/nm), viscosity has negligible effect on cell spreading, as the number of clutches that can be form has reached a plateau due to the elevated ECM rigidity in this case (Fig. 2*A*). The optimum viscosity (for inducing maximized cell spreading) as a function of both the long-term and additional substrate stiffness is given in Fig. 2*C*. In regime *I*, optimal cell spreading is achieved at intermediate levels of viscosity for compliant ECMs, while, in regime *II*,

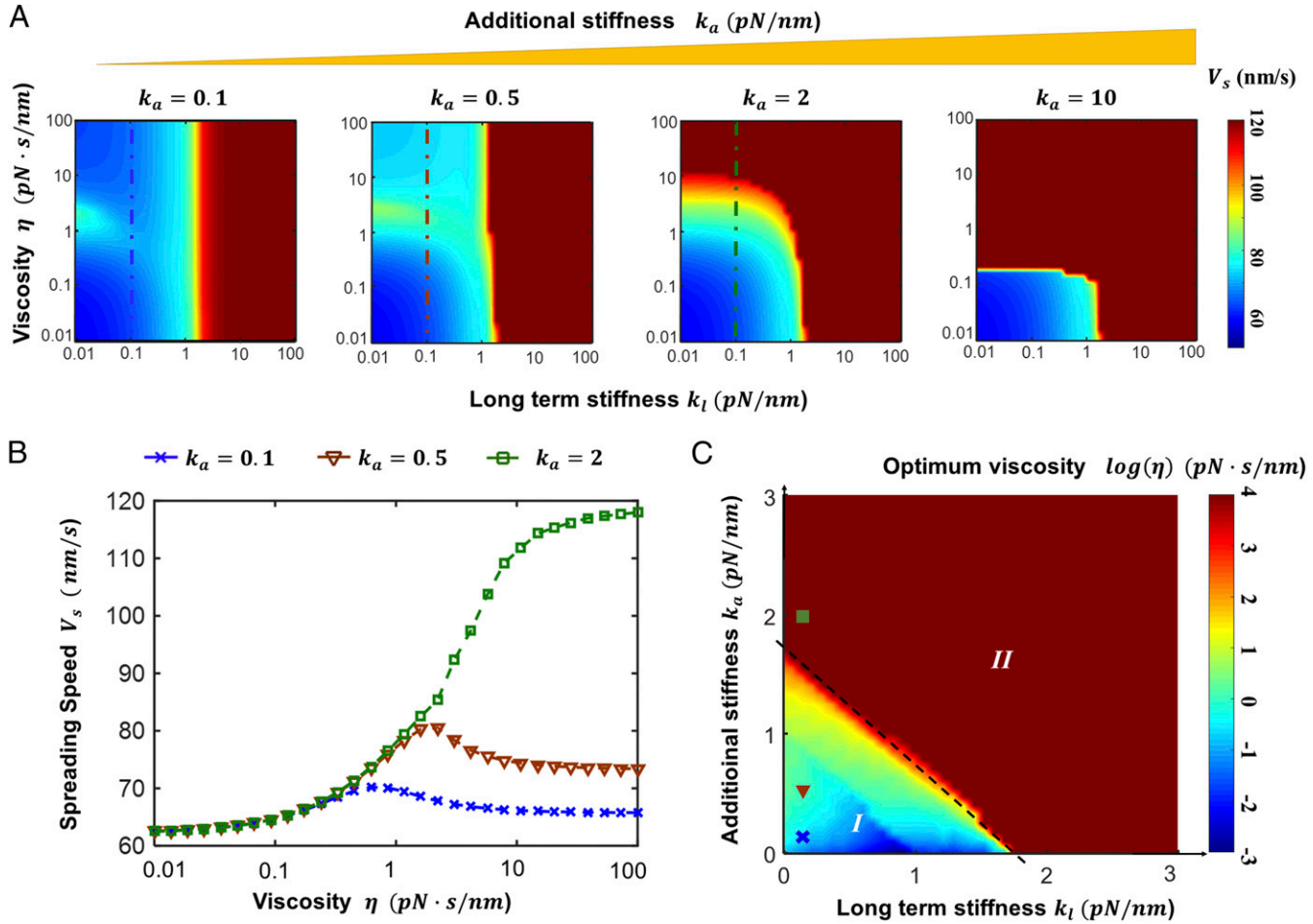

Fig. 2. Cell spreading speed is significantly different based on the elastic and viscous parameters (k_a, k_l, η) of the substrate. (*A*) Heat maps of spreading speed, V_s, plotted as a function of long-term stiffness, k_l, and viscosity, η, from the ODE method. The substrate additional stiffness, k_a, increases from 0.1 pN/nm to 10 pN/nm from *Left* to *Right*. (*B*) Mean spreading speed versus viscosity, η, under different values of k_a (corresponding to the dashed lines in *A*) and a fixed k_l of 0.1 pN/nm. There is an optimum viscosity that maximizes cell spreading, which becomes more significant as k_a increases from 0.1 pN/nm to 0.5 pN/nm. Above k_a = 5 pN/nm, the substrate behaves like a Kelvin–Voigt material with a sharp increase in cell spreading with viscosity. (*C*) The heat map of the optimum viscosity (for inducing maximum spreading speed) plotted as a function of long-term and additional stiffness. The spreading speed is maximized at intermediate viscosity in regime I, while a monotonic increase of the spreading speed with viscosity is observed in regime II. The symbols in *C* correspond to three cases for different k_a in *B*. Based on typical length of FAs (~1 μm), a substrate stiffness of 1 pN/nm is equivalent to a modulus of 1 kPa (*Supporting Information*).

largest spreading occurs when viscosity is large. A summary of how cell spreading is influenced by the elastic and viscous parameters (at low, medium, and high levels) is provided in Fig. S4. In contrast, when there is no clutch reinforcement, cell spreading is suppressed at high ECM stiffness, which leads to frictional slippage behaviors (15) of FAs (*Binding Timescale and the Characteristic Lifetime Dictate the Behavior of FAs*). The corresponding phase diagram in this case is also shown in Fig. S3 for comparison.

Spreading Is Optimal When Substrate Relaxation Timescale Is Comparable to Clutch Binding Timescale. To investigate the optimum in cell spreading that is observed at intermediate viscosities for soft substrates, we analyzed the relevant timescales controlling cell spreading in our model. First, as the clutches attach to the actin filament and stretch, the force they exert on the substrate increases at a rate $v_u k_l$. Therefore, the characteristic time it takes the clutches to develop sufficient force to stall the motors forces ($F_m N_m$) can be identified as $\tau_l = F_m N_m / v_u k_l$. It should be noted that the actual lifetime t_{life} of an FA is proportional to τ_l (*Supporting Information*). Similarly, $\tau_b = 1/r_{on}$ defines the timescale for the clutches to bind, which is also correlated with the formation time (t_{bind}) of the FAs (*Supporting Information*). Depending on the value of the two timescales, the FA cluster exhibits different behaviors that eventually lead to different cell spreading (*Supporting Information*). Finally, the viscoelastic nature of the ECM introduces a characteristic relaxation timescale, $\tau_s = \eta / k_a$. Essentially, upon loading, the effective substrate stiffness decays exponentially (with the timescale τ_s) from its initial value of $k_a + k_l$ to the long-term stiffness, k_l.

Plotting the mean spreading speed as a function of the ratio between the relaxation and binding timescales shows that maximal cell spreading occurs at intermediate viscosity values when the substrate relaxation timescale τ_s is within an order of magnitude of τ_b (Fig. 3*A*). This behavior can be explained by examining the cell spreading that occurs during a single FA lifetime in relation with the three pertinent timescales (τ_b, τ_l, and τ_s).

i) When $\tau_s < \tau_b$, the ECM stiffness relaxes rapidly to its long-term value faster than the clutches can fully bind to the substrate. Consequently, the FAs only sense the long-term stiffness, k_l, and the effect of viscosity becomes negligible. In this case, a typical clutch behavior in one lifetime cycle is shown by the red curve in Fig. 3*C*, which corresponds to the red cross in Fig. 3*B*.

ii) When $\tau_b < \tau_s < \tau_l$, FAs sense a gradual change of stiffness during their formation–disruption cycle. The green curve (Fig. 3*C* corresponding to $\eta = 10^0$ pN·s/nm) shows how the cell spreading speed varies with respect to time. Interestingly, a clear inflection can be seen at around 2 s, demonstrating a change in the effective ECM stiffness. Before 2 s, the cell spreading speed is almost same as that of $\eta = 10^2$ pN·s/nm, suggesting only the initial ECM stiffness is detected by the cell. After the inflection point, cells gradually sense the relaxed stiffness that helps FAs extend their

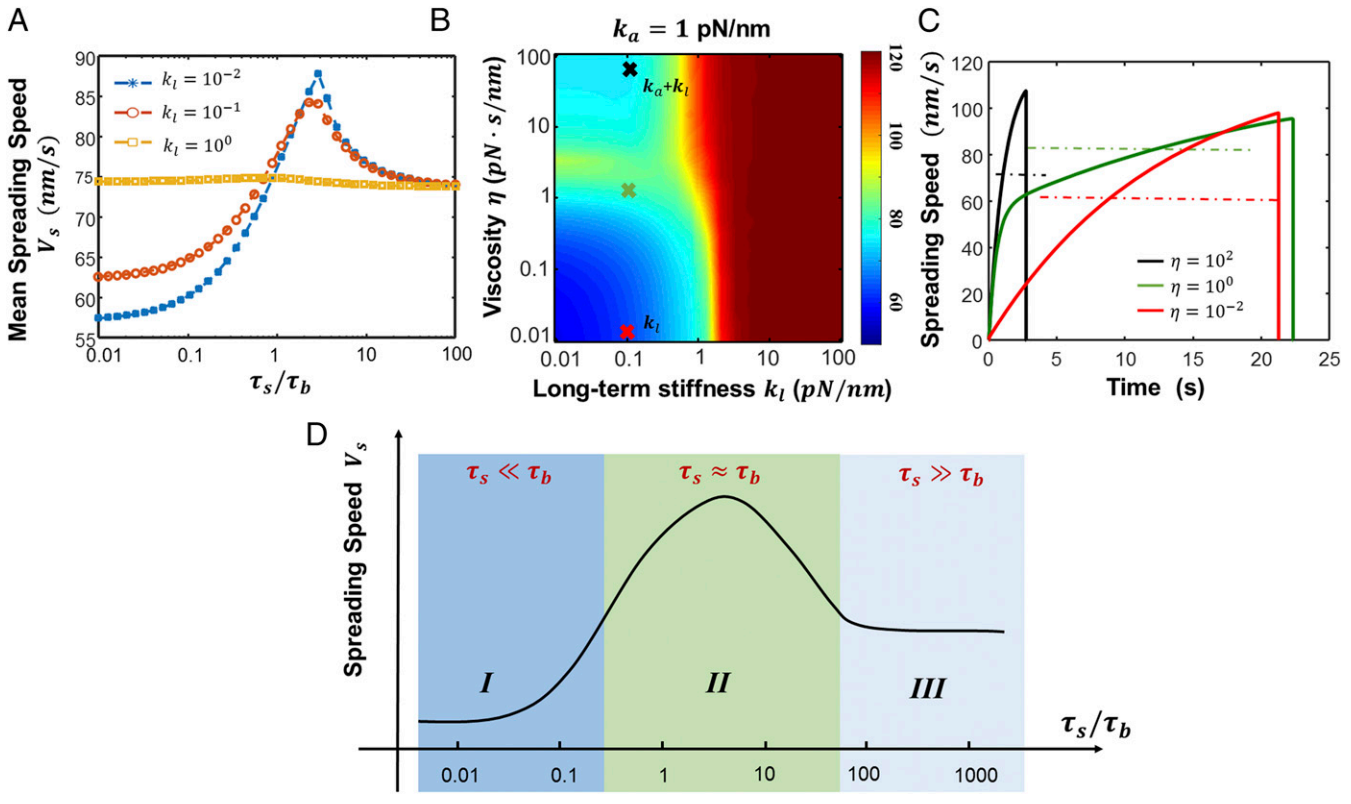

Fig. 3. Optimal substrate viscosity is determined by the ratio between the substrate relaxation (τ_s) and clutch binding (τ_b) timescales. (*A*) Mean spreading speed plotted as a function of τ_s/τ_b for three different values of k_l (with fixed initial stiffness $k_a + k_l = 1.1$ pN/nm) shows that the greatest cell spreading occurs on a substrate where τ_s is slightly greater than τ_b. (*B*) Heat map of spreading speed, V_s, plotted as a function of the long-term stiffness, k_l, and viscosity, η, calculated using the ODE method for $k_a = 1$ pN/nm. (*C*) Spreading speed vs. time for three typical values of η corresponding to the cross points in *B*, with dash-dotted lines representing the time average. The black line represents a highly viscous substrate that relaxes slowly such that the cells only sense the initial substrate stiffness (i.e., $\tau_s > \tau_l > \tau_b$). The red line represents a substrate with low viscosity that relaxes quickly on which cells mainly sense the long-term stiffness (i.e., $\tau_s \ll \tau_b$). The green line represents the optimal viscosity where the substrate relaxes during the FA lifetime (i.e., $\tau_s \approx \tau_b$). (*D*) Schematic of three regimes for effect based on relaxation timescales: (*I*) when $\tau_s \ll \tau_b$, the viscoelastic substrate has the same effect on cell spreading as an elastic substrate with the long-term stiffness k_l; (*II*) when $\tau_s \approx \tau_b$, the maximum spreading is observed on viscoelastic substrates; and (*III*) when $\tau_s \tau_b$, the viscoelastic substrate gives the same spreading speed as an elastic substrate with the initial stiffness $k_a + k_l$.

lifetime corresponding to the long-term stiffness. The net outcome is that actin retrograde flow is suppressed at the beginning while a long FA lifetime is maintained, thereby maximizing cell spreading.

iii) When $\tau_s > \tau_l$, the substrate does not relax during the lifetime of the FA. As such, the ECM behaves elastically, with the effective stiffness $k_a + k_l$. A representative response of an FA in this regime is shown by the black curve in Fig. 3*C*, with a sharp increase in the spreading speed at the beginning, yet a very short lifetime.

Three regimes in Fig. 3*D* show the distinct regulation effects as the relaxation timescales are varied. Note that this only applies for soft substrates; as the long-term stiffness increases, clutch reinforcement mechanism increases the binding rate, saturates bounded clutches, and weakens the viscosity effects. The end effect is that the substrate properties and clutch binding kinetics produce phenomenological timescales that must be precisely tuned so that substrate viscoelasticity has a significant impact on cell spreading. Specifically, for viscosity-based regulation to be significant, the material relaxation timescale τ_s should be larger than (or at least comparable to) the characteristic binding time τ_b of the clutches.

Model Predicts Cells Spreading for Several Different Cell Types Across a Wide Range of Elastic and Viscous Substrate Properties. To test the predictions of our model, we performed cell spreading experiments on viscoelastic substrates synthesized by two different methods (refer to Figs. 4*A* and 5*A*). The measured spreading area and the predicted spreading speed of 3T3 fibroblasts cultured on substrates, fabricated by integrating viscous linear polyacrylamide (5%) in the structure of an elastic cross-linked polyacrylamide network (8%), are shown in Fig. 4*D*. Compared with a purely elastic substrate with the same long-term stiffness, viscosity significantly increased cell spreading (Fig. 4*D*). Interestingly, the same experiment using human mesenchymal stem cells (MSCs) conducted on a different type of viscoelastic substrate, fabricated by combining covalent and supramolecular cross-linking, indicated that viscosity has no significant effect (Fig. 5*D*). To understand the reason behind these differences in cellular response, stress relaxation tests were conducted to characterize the viscoelastic properties of the different substrates (Figs. 4*B* and 5*B*). Time spectrum analysis based on a generalized Maxwell model (see *Methods* and *Extracting Substrate Parameters from Relaxation Test*) revealed the presence of multiple relaxation timescales for the substrates (Figs. 4*C*, *Inset* and 5*C*, Inset). Following analysis of the competition between the lifetime, binding, and relaxation timescales, only the relaxation timescales that are longer than the binding timescale ($\tau_s \geq \tau_b$, i.e., the peaks on the right part of dashed line) play a role in viscosity regulation (Figs. 4*C* and 5*C*). Although these two substrates share similar long-term moduli, the difference in effective relaxation timescales in the two cases puts them into different regimes in the phase diagram. Specifically, substrates fabricated

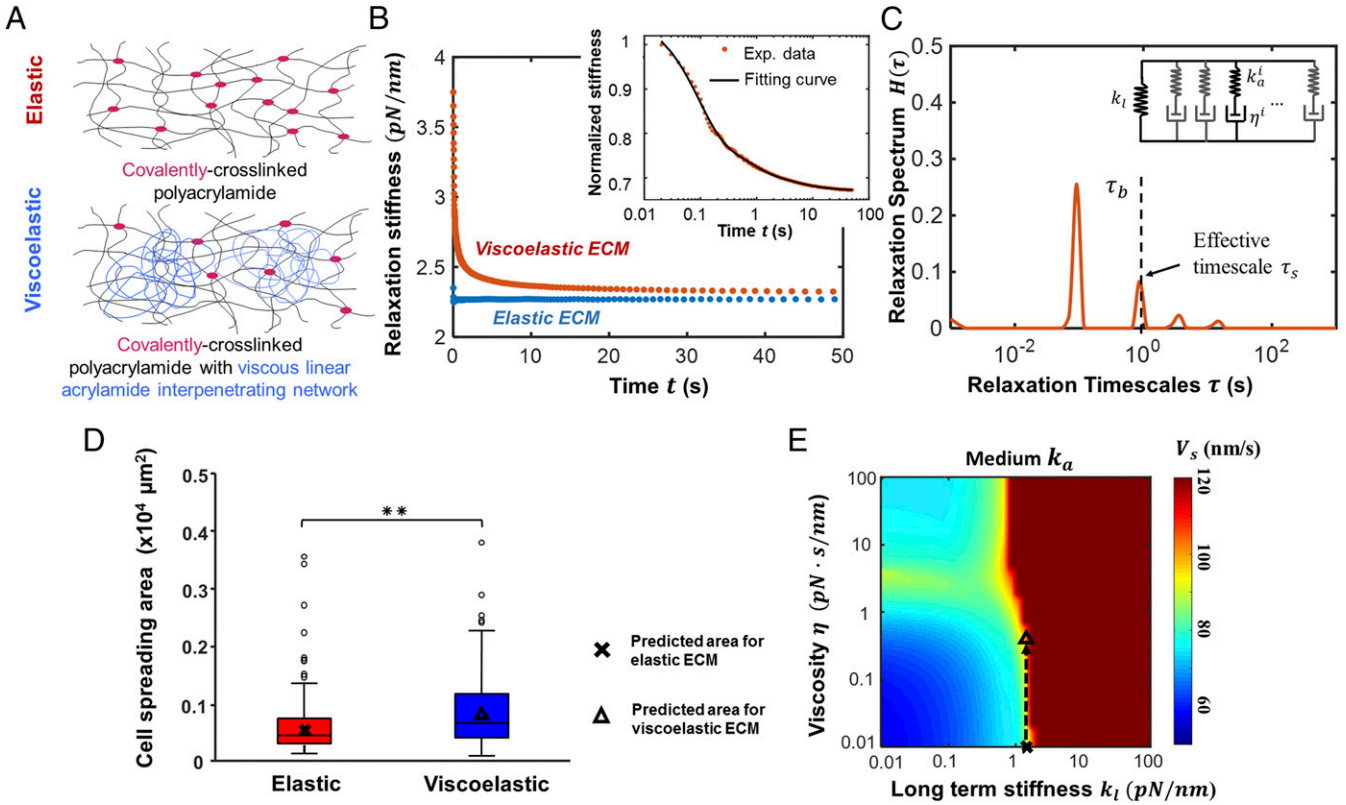

Fig. 4. Model explains that viscosity increases cell spreading for substrates synthesized by combining a network of cross-linked polyacrylamide with linear acrylamide. (*A*) The method used to prepare viscoelastic gels: combining a network of cross-linked polyacrylamide (elastic) with linear polyacrylamide (viscous). (*B*) The relaxation stiffness as a function of time for cross-linked polyacrylamide substrate (elastic, blue dots) and cross-linked polyacrylamide and linear acrylamide substrate (viscoelastic, red dots). (*Inset*) Fitting of the relaxation time spectra (black line) for the normalized stiffness of the viscoelastic substrate (red dot markers). (*C*) Relaxation spectra of the viscoelastic substrate shows that $\tau = 1$ s is the dominant relaxation timescale greater than the binding timescale. (*Inset*) The generalized Maxwell model with multiple relaxation timescales. (*D*) For gels synthesized with this method (*A*), viscosity increases cell spreading 4 h after seeding, where a significant difference (n ≥ 180 cells, $^{**}P < 0.01$, Student's test) is observed. Note that cross and triangle symbols show the simulated cell spreading area on elastic and viscoelastic substrate, respectively. (*E*) The relevant positions are also marked on the heat map of spreading speed for $k_a = 1$ pN/nm. The trend predicted by the model agrees with the experimental cell spreading area.

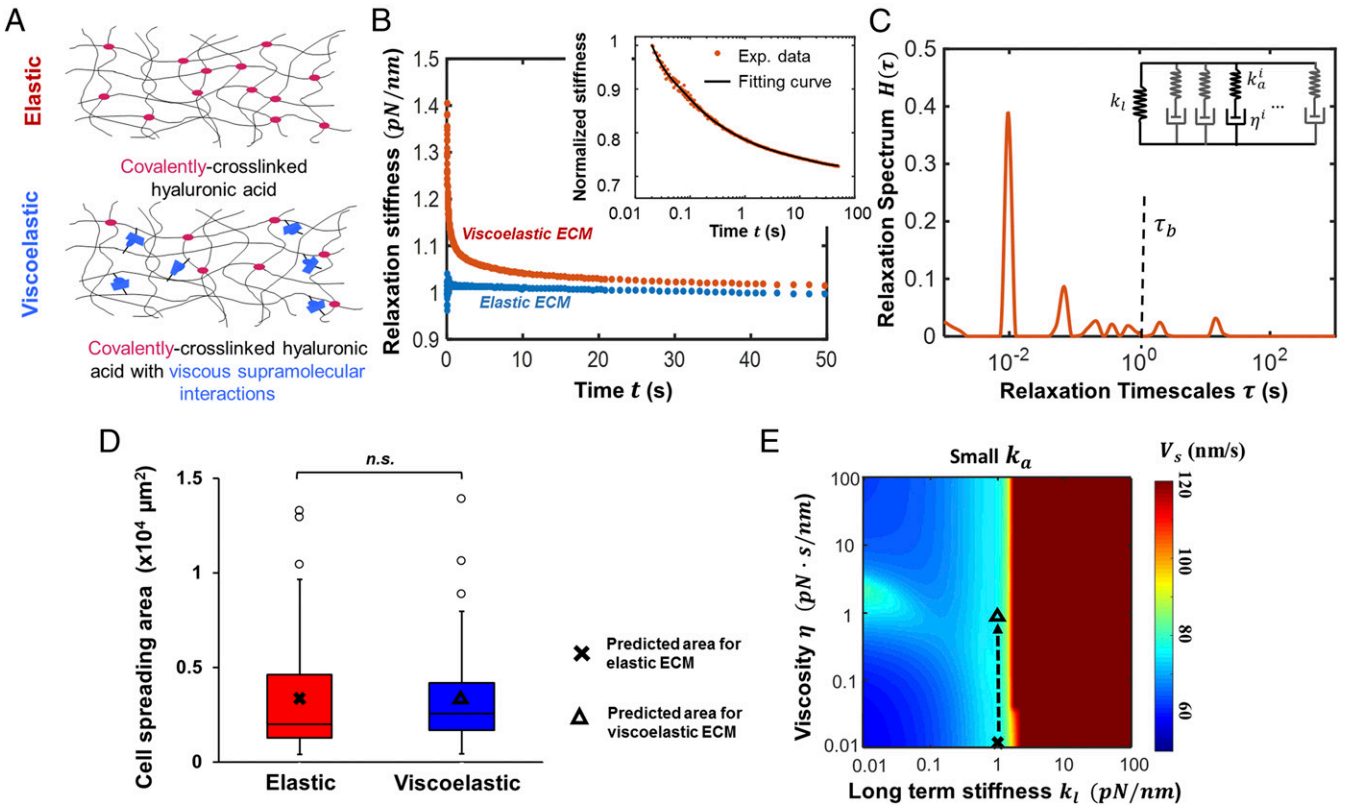

Fig. 5. Model explains that viscosity has no effect on cell spreading for substrates synthesized by combining covalent and supramolecular cross-linkers. (*A*) The method used to prepare viscoelastic gels: combining covalent and supramolecular cross-linkers (see *Methods*). (*B*) The relaxation stiffness as a function of time for covalently cross-linked substrate (elastic, blue dots) and covalent and supramolecular cross-linked substrate (viscoelastic, red dots). (*Inset*) Fitting of the relaxation time spectra (black line) for the normalized stiffness of viscoelastic substrates (red dot markers). (*C*) The relaxation spectrum $H(\tau)$ was plotted as a function of the relaxation timescale τ, which represents (*Inset*) the generalized Maxwell model. There is no apparent relaxation timescale that is larger than (or comparable to) the binding timescale ($\tau_b \approx 1$ s). (*D*) For substrates synthesized with the method in *A*, cell spreading area was similar for elastic and viscoelastic substrates; $n \geq 80$ cells, and n.s. indicates that no statistically significant difference is observed (using the Student's test). Note that cross and triangle symbols show the simulated cell spreading area on elastic and viscoelastic substrate, respectively. (*E*) The relevant positions are also marked on the heat map of spreading speed for $k_a = 0.1$ pN/nm. The trend predicted by the model agrees with the experimental cell spreading area.

with viscoelastic polyacrylamide exhibit a prominent relaxation timescale of $\tau_s \approx 1$ s (Fig. 4*C*). The triangle marker in Fig. 4*E* denotes the position of these viscoelastic material parameters (with the cross marker representing the elastic substrate with the same long-term stiffness) in the heat maps of the predicted spreading speeds. Clearly, cell spreading speed (Fig. 4*E*) and hence spreading area (Fig. 4*D*) are in good agreement with experimental results. In contrast, for substrates prepared from covalent and supramolecular cross-linkers, the relaxation time spectrum indicates there are no prominent peaks (significant relaxation timescales) beyond the characteristic binding time (Fig. 5*C*). By choosing the small peak at $\tau_s \approx 3$ s, simulations indicate that the viscosity of these ECMs has a negligible effect on cell spreading (Fig. 5*D*). Since the additional stiffness is small, when the other small peaks were considered, viscosity still did not influence cell spreading velocity or spreading (Fig. 5 *D* and *E*). In fact, this insignificant effect of viscosity on cell spreading was predicted to be independent of the long-term substrate stiffness (Fig. 5*E*), which was confirmed by our additional experiments on gels that are both softer and stiffer (Fig. S5).

We also compared our model predictions with previous data of U2OS cells seeded on alginate gels that also demonstrated that viscosity promotes cell spreading on soft substrates while reducing spreading on stiff substrates (4) (Fig. 6 *D* and *E*). Time spectrum analysis shows that the effective relaxation timescale of this type of viscoelastic substrate is around 15 s (Fig. S6), indicating that the appearance of viscosity would enhance cell spreading compared with elastic substrate with the same long-term stiffness. However, since the initial stiffness ($k_a + k_l$) was kept constant for the elastic and viscoelastic substrates in that study, the phase diagram has to be replotted accordingly (Fig. S6*C*). The corresponding positions of the experimental configurations are shown on the heat maps for cell spreading in Fig. 6 *A*–*C*. Again, by choosing an appropriate steady spreading timescale, the simulation results fit well with the experimental data (Fig. 6*D*). Note that we also carried out simulations with the generalized Maxwell model that incorporates multiple relaxation timescales to verify the choice of the effective timescale (Fig. S8 and *Simulation with Multiple Relaxation Timescales*).

At this point, we have shown that different observations of viscoelastic regulation are, in fact, attributed to the difference of substrate parameter values. This difference in the parameters leads to the different lifetime and relaxation timescales, which puts the system in a different region in the phase diagram. It must be pointed out that, although we have validated our model with experimental data based on a wide range of parameter values, a large region parameter space remains for further experimental exploration.

Discussion and Conclusions

In summary, we use both analytical and Monte Carlo methods to simulate FA engagement and cell spreading behavior. Rather than using a stochastic lattice model (4), we combined the motor-clutch model with a simple standard linear viscoelastic substrate to

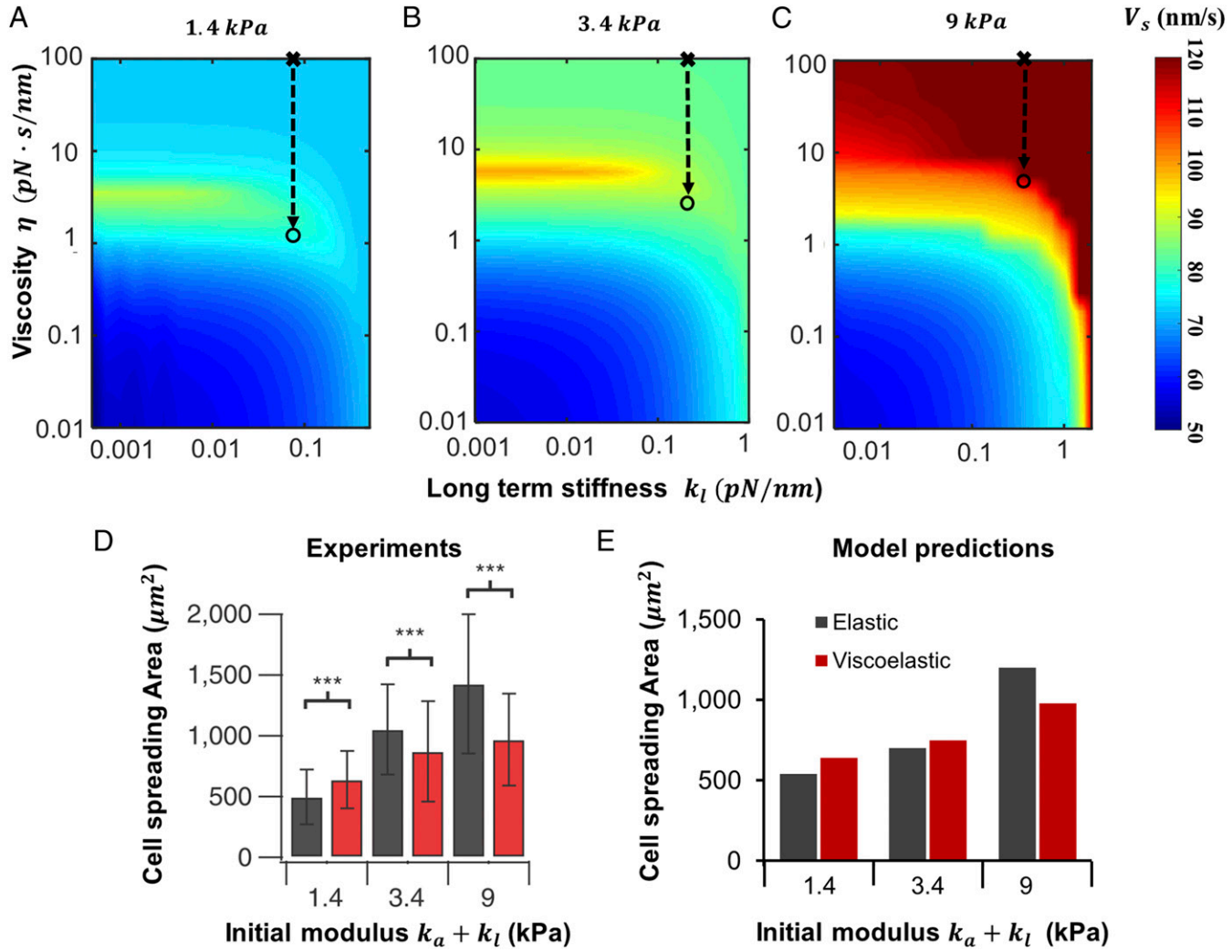

Fig. 6. Model explains experimental findings that viscosity increases cell spreading for low initial stiffness and suppresses cell spreading for high initial stiffness. (*A*–*C*) Heat maps of spreading speed, V_s, plotted as a function of the long-term stiffness, k_l, and viscosity, η, calculated using the ODE method for a fixed initial stiffness of (*A*) 1.4 kPa, (*B*) 3.4 kPa, and (*C*) 9 kPa. Crosses and circles indicate the measured properties of the elastic and viscoelastic substrates used for experiments in ref. 4. (see *Supporting Information* for more details). The viscoelastic relaxation spectrum for this system is given in Fig. S6. (*D*) Quantification of the cell spreading area as a function of the initial moduli of cells on elastic (gray) or viscoelastic (maroon) substrates. Reprinted with permission from ref. 4. Data are shown as mean ± SD, and ***$P < 0.001$ (Student's *t* test). (*E*) Model predictions for cell spreading on elastic (gray) or stress-relaxing (maroon) substrates exhibit a behavior similar to the experimental results, where substrate viscosity leads to an increase in cell spreading at a low initial stiffness and decrease in spreading at high initial stiffness.

show how different viscoelastic material parameters (long-term stiffness, additional stiffness and viscosity) regulate cell spreading. To be specific, at low long-term and additional stiffness, viscosity promotes cell spreading, and maximum cell spreading is achieved at an intermediate viscosity value. In contrast, viscosity has a negligible effect on spreading when the long-term stiffness is large. This insensitivity of cell spreading on viscosity in this regime stems from the clutch reinforcement effect that leads to a saturation of the bounded clutches that can be formed on stiff ECMs. However, such a reinforcing mechanism (under high clutch load) may not be present in certain cell types, like neurons (32, 33), which eventually leads to suppressed cell spreading when the substrate becomes very rigid. The effect of viscosity for these cell types is presented in *Supporting Information*.

Timescale analysis revealed that substrate viscoelasticity regulates cell spreading based on the magnitude of the substrate relaxation timescale compared with the timescales of motor clutch binding and FA lifetime. The clutch binding time (τ_b) is solely due to the stochastic binding nature of FA molecules (e.g., integrins, talin, vinculin) with value of ∼1 s (15, 16). The interaction between the pulling force of myosin motors and the substrate stiffness yields an FA lifetime timescale (τ_l) in the range of 10^{-1} s to 10^3 s. When reinforcement does not take effect, the FA lifetime is proportional to its lifetime timescale, τ_l (16). The average lifetime is ∼10 s to 100 s depending on the stiffness, which conforms with nascent FAs within the lamellipodium (34). However, once the reinforcement takes effect, the FA lifetime can be in minutes or even longer (divergent case), which is consistent with many experiments showing stable FAs for stiffer substrates (1, 9, 35). The substrate relaxation timescale (τ_s) would span a wide range of 10^{-2} s to 10^2 s, corresponding to the viscoelastic nature of different substrate. The relationship between the three timescales (τ_l, τ_b, τ_s) clearly explains how viscosity regulates cell spreading. The regulation effect based on the timescales analysis is summarized in Fig. 7. Specifically, when $\tau_l > \tau_b$, cell spreading is greatest when the relaxation timescale τ_s falls between the binding timescale τ_b and the lifetime timescale τ_l ($\tau_b < \tau_s < \tau_l$); when $\tau_l < \tau_b$, clutch reinforcement takes effect and

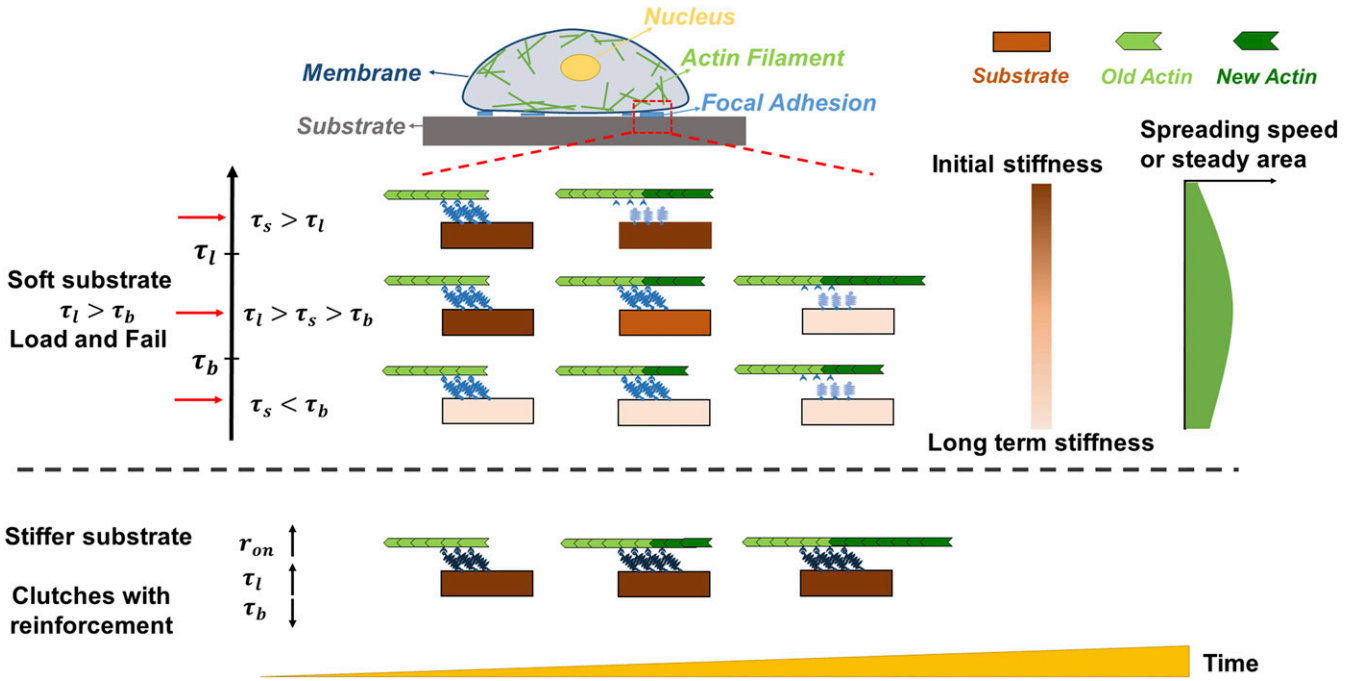

Fig. 7. Optimal viscosity minimizes actin retrograde flow while maximizing FA lifetime for soft substrates. Schematic describes effects of substrate viscoelasticity on cellular behavior based on the comparison of the clutch binding timescale, τ_b, substrate relaxation timescale, τ_s, and lifetime scale, τ_l. In the load and fail region ($\tau_l > \tau_b$), cell spreading is maximized when $\tau_l > \tau_s > \tau_b$ such that the cells experience a substrate with a high initial stiffness that relaxes shortly after initial clutch engagement. This minimizes actin retrograde flow while maintaining a long FA lifetime, thereby maximizing cell spreading. When the substrate viscosity is too low (i.e., $\tau_s < \tau_b$), cells only sense the long-term stiffness, which provides a long FA lifetime without restricting actin retrograde flow. When the substrate viscosity is too high (i.e., $\tau_s > \tau_l$), the cells only sense the high initial stiffness that doesn't diminish during the FA lifetime, causing the clutches to prematurely fail. In comparison, for stiff ECMs, a large number of clutches will be formed due to clutch reinforcement, leading to an increased FA lifetime that limits the retrograde flow and enhances the spreading speed.

leads to saturation of the cell spreading area; in this case, viscosity has no effect on cell spreading. The relaxation timescales that are smaller than binding timescale ($\tau_s < \tau_b$) have a negligible effect on cell spreading.

We also developed a practical way to determine the effective relaxation timescale of viscoelastic substrate regarding the influence on cell spreading. First, relaxation time spectra (Figs. 4*C* and 5*C* and Fig. S6) were obtained from stress relaxation data of viscoelastic substrates. Then, we picked the most significant timescale (i.e., the highest peak for $\tau_s \geq \tau_b$) from relaxation spectrum as the effective timescale. Explicit simulations with multiple timescales confirmed that our choice of the effective timescale faithfully describes the dynamics cell spreading (Fig. S8 and *Simulation with Multiple Relaxation Timescales*) on viscoelastic substrates. In cases where there are multiple prominent relaxation times beyond the binding timescale, simulations show that the resulting cell spreading is approximately a weighted average of the effect for each timescale.

Previous studies suggested that the effects of substrate viscoelasticity on cell spreading are due to local substrate densification and plastic flow (4). However, these experimental results can be reproduced by our model (Fig. 6), demonstrating that viscoelasticity alone is capable of explaining their findings. It is important to note that our model successfully explains the viscoelastic regulation of cell spreading for three completely distinct types of hydrogels [hyaluronic acid (HA), polyacrylamide, alginate] with different ways of imparting viscoelasticity (supramolecular interactions, semiinterpenetrating network/entanglements, ionic cross-linking), different stiffnesses (range from 10^{-1} pN/nm to 10^{1} pN/nm), and different cell types (human MSCs, 3T3 fibroblasts, U2OS osteosarcoma line). In addition, our experiments using substrates produced with different fabrication methods (and exhibiting virtually no plasticity) are also consistent with the model predictions. While these results demonstrate that viscoelasticity alone has a strong influence on cell spreading, plasticity and ECM remodeling may be equally important. A more complex model that includes plastic theory should be considered in future work.

In conclusion, we have developed an analytical model that incorporates the viscoelastic relaxation time spectrum and successfully explains the effects of substrate viscoelasticity on cell spreading. Our model can be used as a theoretical tool for further study of the viscoelastic regulation of cell behavior for various cell types and tissues. It can also help predict cell spreading over the full parameter space for viscoelastic substrates, which will enable the rational design of biomaterials. Overall, our work provides both physical insight and a practical method to investigate how cellular and material timescales intersect to regulate the cell behavior.

Methods

HA Modification. Norbornene-modified HA (NorHA) was synthesized by amidation with 5-norbornene-2-methylamine (TCI America) and (benzotriazol-1-yloxy) Tris-(dimethylamino) phosphonium hexafluorophosphate (BOP; Sigma) under nitrogen at room temperature for 2 h. NorHA was further modified with adamantane groups (AdNorHA) as previously described (36) to permit supramolecular interactions in viscoelastic HA hydrogels via esterification with 1-adamantane acetic acid (TCI America), 4-(dimethylamino)pyridine (Sigma), and ditertbutyl dicarbonate (Boc_2O; Sigma) under nitrogen at 45 °C for 20 h. The β-cyclodextrin-modified HA (CDHA) was synthesized as previously described (36) to enable supramolecular interactions with adamantane groups on AdNorHA. Briefly, an amine-functionalized cyclodextrin [6-(6-aminohexyl)amino-6-deoxy-β-cyclodextrin] was synthesized (36) and coupled to carboxylic acids on HA using the BOP-mediated amidation protocol described for NorHA above. All reactions were quenched with cold water, purified via dialysis (Spectra/Por, 6- to 8-kDa molecular weight cutoff) and filtration for 7 d at room temperature, frozen, and lyophilized.

HA Hydrogel Fabrication and Rheological Characterization. NorHA elastic hydrogels with covalent cross-linking only were fabricated via UV light-mediated thiol–ene addition (37). NorHA hydrogels were photopolymerized (2 mW·cm^{-2}) in the presence of 1 mM lithium acylphosphinate (38, 39) photoinitiator for 2 min along with thiolated RGD (1 mM, GCGYG*RGD*SPG; GenScript) to permit cell attachment and DTT (Sigma) to promote covalent cross-linking. AdNorHA–CDHA viscoelastic hydrogels with both covalent and supramolecular cross-links were fabricated similarly to the NorHA elastic hydrogels, with AdNorHA and CDHA mixed to promote Ad–CD guest–host interactions followed by thiol–ene photopolymerization. All hydrogels were fabricated between untreated and thiolated (37) coverslips (50 μL, 18 × 18 mm) to make films with ∼100-μm thickness. HA hydrogel stress relaxation properties were assessed using an AR2000ex rheometer (TA Instruments) equipped with a cone and plate geometry (1°, 20 mm diameter) at a 10% applied strain for 5 min.

MSC Cell Culture and Spreading Analysis on HA Hydrogels. Human bone marrow-derived MSCs (Lonza) were used at passage 3 for all experiments. Culture media was composed of α-MEM supplemented with 16.7 vol/vol% FBS (Gibco), 1 vol/vol% penicillin streptomycin (Invitrogen), 1 vol/vol% L-glutamine (Invitrogen), and 1 vol/vol% fungizone amphotericin B (Invitrogen). All polymer, peptide, and cell culture reagents were either sterile-filtered or sterilized via germicidal UV irradiation before cell culture. MSCs were seeded atop hydrogel thin films (18 × 18 mm) in six-well plates at a density of 2×10^3 cells/cm^2 and cultured for 2 d. Phase contrast images of MSCs atop HA hydrogels were acquired on a Zeiss Axiovert 200 inverted microscope (Hitech Instruments, Inc.), and spread area was quantified for at least 80 cells per experimental group using National Institutes of Health (NIH) ImageJ.

The 3T3 Fibroblast Cells Culture. The 3T3 NIH cells (ATCC) were maintained in DMEM (Gibco) supplemented with 10% FBS (ATCC) and 1% penicillin streptomycin (Gibco) at 37 °C and 5% CO_2. Cells were suspended with trypsin 0.05% and plated on gels. The projected area of single fibroblasts was manually quantified 4 h after plating, on bright field images taken with a LEICA II inverted microscope with a 10× objective.

Viscoelastic Polyacrylamide Gels Fabrication and Rheological Characterization. A 5% (wt/vol) acrylamide solution is polymerized without bis-acrylamide. The resulting linear polyacrylamide molecules are entrapped in a network made of 8% (wt/vol) acrylamide and 0.125% (wt/vol) bis-acrylamide. This hydrogel is sterilized by a 15-min exposure to germicidal UV light, and activated by immersion in a sulfosuccinimidyl 6-(4′-azido-2′-nitrophenylamino)hexanoate solution in Hepes 50 mM, pH = 8.2 and exposed to UV for 8 min. The surface of gels is functionalized with a 2-h RT incubation with 50 μg/mL of rat-tail collagen I (Corning) in Hepes 50 mM pH = 8.2. The resulting gel presents collagen I cross-linked to both the linear and the networked polyacrylamide. The rheology of polyacrylamide gels was characterized with a Kinexus rheometer (Malvern) using parallel plate geometry (20 mm in diameter plate). The polyacrylamide gels display the typical behavior of viscoelastic solids as quantified with stress relaxation experiments (strain = 0.1).

Numerical Methods and Time Spectrum Analysis. We use both KMC based on Gillespie algorithm and analytical solution by solving ODE to simulate the process of cell spreading. The relaxation time spectrum was obtained from the stress relaxation data through the regularized Inverse Laplace Transformation (40). All simulations and analysis were carried out in MATLAB; details can be found in *Supporting Information*.

1. Trichet L, et al. (2012) Evidence of a large-scale mechanosensing mechanism for cellular adaptation to substrate stiffness. *Proc Natl Acad Sci USA* 109:6933–6938.
2. Shenoy VB, Wang H, Wang X (2016) A chemo-mechanical free-energy-based approach to model durotaxis and extracellular stiffness-dependent contraction and polarization of cells. *Interface Focus* 6:20150067.
3. Sunyer R, et al. (2016) Collective cell durotaxis emerges from long-range intercellular force transmission. *Science* 353:1157–1161.
4. Chaudhuri O, et al. (2015) Substrate stress relaxation regulates cell spreading. *Nat Commun* 6:6364.
5. Nisenholz N, et al. (2014) Active mechanics and dynamics of cell spreading on elastic substrates. *Soft Matter* 10:7234–7246.
6. Klein EA, et al. (2009) Cell-cycle control by physiological matrix elasticity and in vivo tissue stiffening. *Curr Biol* 19:1511–1518.
7. Trappmann B, et al. (2012) Extracellular-matrix tethering regulates stem-cell fate. *Nat Mater* 11:642–649.
8. Swift J, et al. (2013) Nuclear lamin-A scales with tissue stiffness and enhances matrix-directed differentiation. *Science* 341:1240104.
9. Cao X, et al. (2015) A chemomechanical model of matrix and nuclear rigidity regulation of focal adhesion size. *Biophys J* 109:1807–1817.
10. Parsons JT, Martin KH, Slack JK, Taylor JM, Weed SA (2000) Focal adhesion kinase: A regulator of focal adhesion dynamics and cell movement. *Oncogene* 19:5606–5613.
11. Plotnikov SV, Pasapera AM, Sabass B, Waterman CM (2012) Force fluctuations within focal adhesions mediate ECM-rigidity sensing to guide directed cell migration. *Cell* 151:1513–1527.
12. Shemesh T, Geiger B, Bershadsky AD, Kozlov MM (2005) Focal adhesions as mechanosensors: A physical mechanism. *Proc Natl Acad Sci USA* 102:12383–12388.
13. Case LB, Waterman CM (2015) Integration of actin dynamics and cell adhesion by a three-dimensional, mechanosensitive molecular clutch. *Nat Cell Biol* 17:955–963.
14. Cao X, et al. (2017) Multiscale model predicts increasing focal adhesion size with decreasing stiffness in fibrous matrices. *Proc Natl Acad Sci USA* 114:E4549–E4555.
15. Chan CE, Odde DJ (2008) Traction dynamics of filopodia on compliant substrates. *Science* 322:1687–1691.
16. Bangasser BL, Odde DJ (2013) Master equation-based analysis of a motor-clutch model for cell traction force. *Cell Mol Bioeng* 6:449–459.
17. Bangasser BL, Rosenfeld SS, Odde DJ (2013) Determinants of maximal force transmission in a motor-clutch model of cell traction in a compliant microenvironment. *Biophys J* 105:581–592.
18. Ghassemi S, et al. (2012) Cells test substrate rigidity by local contractions on submicrometer pillars. *Proc Natl Acad Sci USA* 109:5328–5333.
19. Étienne J, et al. (2015) Cells as liquid motors: Mechanosensitivity emerges from collective dynamics of actomyosin cortex. *Proc Natl Acad Sci USA* 112:2740–2745.
20. Elosegui-Artola A, et al. (2016) Mechanical regulation of a molecular clutch defines force transmission and transduction in response to matrix rigidity. *Nat Cell Biol* 18:540–548.
21. Elosegui-Artola A, et al. (2014) Rigidity sensing and adaptation through regulation of integrin types. *Nat Mater* 13:631–637.
22. Roberts WW, Kramer O, Rosser RW, Nestler FHM, Ferry JD (1974) Rheology of fibrin clots. I. Dynamic viscoelastic properties and fluid permeation. *Biophys Chem* 1:152–160.
23. Deng L, et al. (2006) Fast and slow dynamics of the cytoskeleton. *Nat Mater* 5:636–640.
24. Alcaraz J, et al. (2003) Microrheology of human lung epithelial cells measured by atomic force microscopy. *Biophys J* 84:2071–2079.
25. Verdier C, Etienne J, Duperray A, Preziosi L (2009) Review: Rheological properties of biological materials. *C R Phys* 10:790–811.
26. Cameron AR, Frith JE, Cooper-White JJ (2011) The influence of substrate creep on mesenchymal stem cell behaviour and phenotype. *Biomaterials* 32:5979–5993.
27. Bell GI (1978) Models for the specific adhesion of cells to cells. *Science* 200:618–627.
28. Mogilner A, Oster G (1996) Cell motility driven by actin polymerization. *Biophys J* 71:3030–3045.
29. Alberts B (2008) *Molecular Biology of the Cell* (Garland Sci, New York).
30. Giannone G, et al. (2004) Periodic lamellipodial contractions correlate with rearward actin waves. *Cell* 116:431–443.
31. Jurado C, Haserick JR, Lee J (2005) Slipping or gripping? Fluorescent speckle microscopy in fish keratocytes reveals two different mechanisms for generating a retrograde flow of actin. *Mol Biol Cell* 16:507–518.
32. Koch D, Rosoff WJ, Jiang J, Geller HM, Urbach JS (2012) Strength in the periphery: Growth cone biomechanics and substrate rigidity response in peripheral and central nervous system neurons. *Biophys J* 102:452–460.
33. Swaminathan V, Waterman CM (2016) The molecular clutch model for mechanotransduction evolves. *Nat Cell Biol* 18:459–461.
34. Choi CK, et al. (2008) Actin and alpha-actinin orchestrate the assembly and maturation of nascent adhesions in a myosin II motor-independent manner. *Nat Cell Biol* 10:1039–1050.
35. Walcott S, Kim DH, Wirtz D, Sun SX (2011) Nucleation and decay initiation are the stiffness-sensitive phases of focal adhesion maturation. *Biophys J* 101:2919–2928.
36. Rodell CB, Kaminski AL, Burdick JA (2013) Rational design of network properties in guest-host assembled and shear-thinning hyaluronic acid hydrogels. *Biomacromolecules* 14:4125–4134.
37. Gramlich WM, Kim IL, Burdick JA (2013) Synthesis and orthogonal photopatterning of hyaluronic acid hydrogels with thiol-norbornene chemistry. *Biomaterials* 34:9803–9811.
38. Majima T, Schnabel W, Weber W (1991) Phenyl-2,4,6-trimethylbenzoylphosphinates as water-soluble photoinitiators. Generation and reactivity of O=Ṗ(C6H5)(O–) radical anions. *Makromol Chem* 192:2307–2315.
39. Fairbanks BD, Schwartz MP, Bowman CN, Anseth KS (2009) Photoinitiated polymerization of PEG-diacrylate with lithium phenyl-2,4,6-trimethylbenzoylphosphinate: Polymerization rate and cytocompatibility. *Biomaterials* 30:6702–6707.
40. Provencher SW (1982) CONTIN: A general purpose constrained regularization program for inverting noisy linear algebraic and integral equations. *Comput Phys Commun* 27:229–242.